Electronic Spillover from a Metallic Nanoparticle

Can Simple Electrochemical Electron Transfer Processes Be Catalyzed by Electronic Coupling of a Molecular Scale Gold Nanoparticle Simultaneously to the Redox Molecule and the Electrode?

Shermukhamedov, Shokirbek A; Nazmutdinov, Renat R; Zinkicheva, Tamara T; Bronshtein, Michael D; Zhang, Jingdong; Mao, Bingwei; Tian, Zhongqun; Yan, Jiawei; Wu, De-Yin; Ulstrup, Jens

Published in:
Journal of the American Chemical Society

Link to article, DOI:
10.1021/jacs.9b09362

Publication date:
2020

Document Version
Version created as part of publication process; publisher's layout; not normally made publicly available

JACS
JOURNAL OF THE AMERICAN CHEMICAL SOCIETY
pubs.acs.org/JACS
Article

Electronic Spillover from a Metallic Nanoparticle: Can Simple Electrochemical Electron Transfer Processes Be Catalyzed by Electronic Coupling of a Molecular Scale Gold Nanoparticle Simultaneously to the Redox Molecule and the Electrode?

Shokirbek A. Shermukhamedov, Renat R. Nazmutdinov,* Tamara T. Zinkicheva, Michael D. Bronshtein, Jingdong Zhang, Bingwei Mao, Zhongqun Tian, Jiawei Yan, De-Yin Wu, and Jens Ulstrup*

Cite This: https://dx.doi.org/10.1021/jacs.9b09362

ABSTRACT: Electrochemical electron transfer (ET) of transition metal complexes or redox metalloproteins can be catalyzed by more than an order of magnitude by molecular scale metallic nanoparticles (NPs), often rationalized by concentration enhancement of the redox molecules in the interfacial region, but collective electronic AuNP array effects have also been forwarded. Using DFT combined with molecular electrochemical ET theory we explore here whether a single molecular scale Au nanocluster (AuC) between a Au (111) surface and the molecular redox probe ferrocene/ferricinium (Fc/Fc^+) can trigger an ET rate increase. Computational challenges limit us to Au_nCs (n up to 147), which are smaller than most electrocatalytic AuCs studied experimentally. AuC-coating thiols are addressed both as adsorption of two S atoms at the structural Au_{55} bridge sites and as superexchange of variable-size AuCs via a single six-carbon alkanethiyl bridge. Our results are guiding, but enable comparing many AuC surface details (apex, ridge, face, direct vs superexchange ET) with a planar Au(111) surface. The rate-determining electronic transmission coefficients for ET between Fc/Fc^+ and AuC are highly sensitive to subtle AuC electronic features. The transmission coefficients mostly compete poorly with direct Fc/Fc^+ ET at the Au(111) surface, but Fc/Fc^+ 100 face-bound on Au_{79} and Au_{147} and ridge bound on Au_{19} leads to a 2- or 3-fold rate enhancement, in different distance ranges. Single AuCs can thus indeed cause rate enhancement of simple electrochemical ET, but additional, possibly collective AuNC effects, as well as larger clusters and more complete coating layers, also need to be considered.

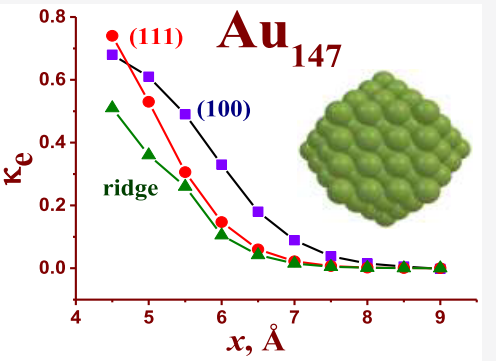

1. INTRODUCTION

Metallic nanoparticles (NPs) protected by organic molecular monolayers are central in contexts ranging from single-molecule "electronics" and molecular wiring[1−4] to biomolecular markers[1,3,5] and electronic relays in interfacial electrochemical and bioelectrochemical catalysis.[5−16] AuNPs have been a core target, but silver, iron, cobalt, platinum, and other metallic NPs[17−20] as well as metal alloys and core−shell NPs[21] have also attracted attention. Variable-size AuNPs have been targets in comprehensive experimental[1−21] and theoretical[14,22−27] studies of electronic AuNP properties. AuNPs that are 1−2 nm coated nanoparticles display single-ET (SET) charging with a Coulomb blockade in both organic[28,29] and aqueous electrolyte solution.[30−32] Similar effects were observed for thiol-roughened planar electrochemical Au surfaces.[33] Electrochemical (*in situ*) scanning tunneling microscopy (STM) offers a further platform for AuNP SET in condensed matter environments.[30−32,34] Electrochemical SET fades out when the NP size exceeds about 2.5 nm,[23,24] i.e., the size range of large transition metal complexes or small redox metalloproteins. Contrary to the molecular targets, the electronic structure of the metallic NPs in this size range approaches a continuum, but still displays catalytic enhancement by an order of magnitude or more in simple electrochemical and bioelectrochemical ET processes.[6−9,11−14]

NP catalysis of gas phase reactions where small molecules are adsorbed on surface facets, kinks, and corners has been framed by electronic structure computations.[5,35,36] Electrocatalysis of simple ET reactions by thiol-protected AuNPs is different, illustrated by the electrocatalysis of transition metal complexes such as $[Fe(CN)_6]^{3-/4-}$,[6,7] quinones,[10] and the redox metalloproteins cyt c[8,9,13] and azurin.[14] In spite of ET distance extension by up to several nanometers, more than an

Received: September 13, 2019
Published: May 20, 2020

order of magnitude rate constant *increase* is observed. Similar extended molecular matter would virtually close the ET channel, reflecting the quite different electronic properties of metallic NPs and "normal" molecular matter. The electrochemical interface is much more complex than the ultrahigh-vacuum NP environment.[37,38] The target molecules are complex and only weakly bound to the AuNP. There is presently no obvious single physical origin of the ET rate enhancement. Electronic structure computations of NPs that include both the electrochemical interface and the solvent, as well as complex redox molecules, are not available either, but "coarse-grained" approaches in condensed matter charge transfer[39,40] and *in situ* STM theory[41−44] introduced early[45−48] may offer clues.

In this study we explore whether insertion of a molecular scale AuNP, hereafter denoted as a Au nanocluster (AuC), between a target reactant molecule, here the ferrocene/ferricinium (Fc/Fc^+) couple, and a Au(111) surface can lead to electrochemical ET rate enhancement. Due to computational challenges, we could not address full 1.5−5 nm AuNPs, but AuCs up to Au_{147} (1.7 nm) are addressed, and the solvent is included. Our study is therefore guiding with a focus on AuC size and surface structure, and on AuC-mediated ET versus direct ET. Specifically we consider the electronic transmission coefficient between Fc/Fc^+ and the electrode surface via a molecular size AuC. We address two "elementary" catalytic mechanisms. AuC catalysis in long-range ET can be regarded as a single coherent resonance tunneling process via a virtual (quasi-)continuous AuC electronic manifold.[14,18] A second view is sequential two-step ET with full excess electron or hole vibrational relaxation in the solvated AuC.[14,18,32,34] We have found that sequential two-step ET is competitive with direct single-step ET between the molecule and the electrode, whereas fully coherent two-step ET is not. We shall compate these single-AuC catalytic views with the collective AuC view of Chavalziel and Allongue[49] in Section 4.

We focus first on an uncoated single molecular scale Au_nC (n = 13−147), specifically the transmission coefficient for ET between the Au_nC and Fc/Fc^+, to explore whether stronger electronic overlap ("spillover") than at a planar Au(111) surface can cause a rate increase. Surface charge dependent electronic density spillover has been discussed in the context of surface plasmon behavior,[22] electrons in alkali metal clusters,[50] surface Raman scattering,[51] size-dependent NP work functions,[52,53] and interfacial electrochemical ET.[54−57] The electronic density beyond the AuC ionic core thus expands differently from a planar surface[50−53] and depends on both the AuC size and electronic surface charge. We combine electronic "spillover" views with the theory of molecular electrochemical ET processes.[39,40] We overview first some formal elements of two-step electrochemical ET via variable-size AuCs compared to direct ET. In coherent two-step ET electronic levels in the "quasi-continuous" AuC level distribution couples, purely electronically, levels around the electrode Fermi level to the vibrationally activated molecular redox level. ET rate enhancement would then arise *either* by energy resonance between the electrode and the AuC levels *or* by enhanced electronic coupling between the redox molecule and the AuC. The rate enhancement in incoherent two-step ET can only be caused by the second effect, i.e., by stronger electronic charge delocalization from the AuC than from the planar electrode surface.

We illustrate the single-AuC electronic effects in two ways. We exploit first the spherical free-electron model. Although crude, this model illuminates size-dependent electronic structural effects. This is followed by DFT computations of the AuC electronic structure and the transmission coefficients for rate-determining ET between Fc/Fc^+ and the $Au_{13-147}Cs$. ET between Fc/Fc^+ and a planar Au surface is a reference. As noted, these clusters are smaller than for reported ET electrocatalysis, but enable illuminating size and surface structure effects.

We mimic, second, the effects of thiol coating by studying both the electronic structure effects of adsorption of two S atoms at the structural Au_{55} bridge sites on the AuC and of superexchange ET between Fc/Fc^+ and variable-size AuCs via a single 6C alkanethiyl bridge. Our conclusion is first that electronic effects of a single AuC can indeed contribute to AuC catalysis, but within the models used, only by a 2- to 3-fold rate enhancement. The transmission coefficients are highly sensitive to the AuC atomic surface structure, with intriguing distance dependences, and with Fc/Fc^+ face(100) binding to Au_{147} and ridge binding to Au_{19} (at short distances) as the only configurations triggering electrocatalysis. We found, second, that the efficiency of bridge-assisted ET via the 6C alkanethiyl bridge can be competitive or exceed the direct ET channel.

2. FORMAL SCHEME FOR DIRECT AND AuC-MEDIATED ELECTROCHEMICAL ET

Figure 1, top, shows a redox molecule (the purple sphere, here Fc/Fc^+) linked to a planar electrode via a bifunctional alkanethiol linking Fc/Fc^+ through the thiyl group (the small yellow sphere) to the (Au) surface. Figure 1, bottom, shows the redox molecule linked via a AuC (large yellow sphere). The linker molecules are comparable in length, as this is representative for the experimental studies.

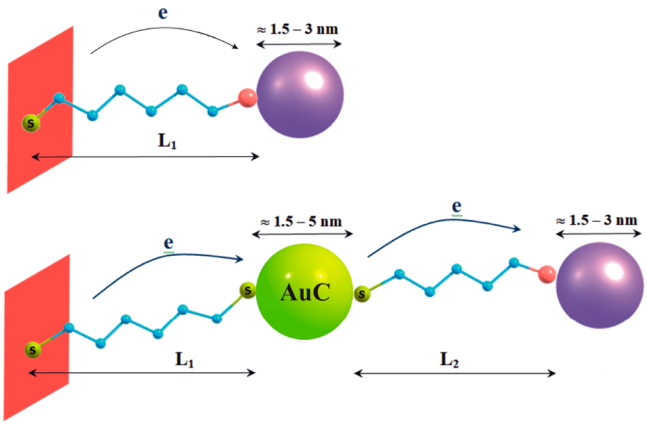

Figure 1. Top: Schematic view of a redox molecule (purple sphere) linked to an electrode surface via a bifunctional alkanethiol linker. The functional groups are represented by the small spheres. Bottom: The redox molecule linked via a AuC.

2.1. Direct Electrochemical Electron Transfer. The following general form of the current i (here cathodic)[39,40] is a suitable reference

https://dx.doi.org/10.1021/jacs.9b09362
J. Am. Chem. Soc. XXXX, XXX, XXX−XXX

$$i = e\int_{-\infty}^{\infty} f(\varepsilon)\rho(\varepsilon)W(\varepsilon;\eta)\mathrm{d}\varepsilon \approx e\rho(\varepsilon_F)[T(\varepsilon_F)]^2\sqrt{\frac{\pi}{E_r k_B T\hbar^2}}\int_{-\infty}^{\infty} f(\varepsilon)\exp\left\{-\frac{[E_r - e\eta - \varepsilon]^2}{4E_r k_B T}\right\}\mathrm{d}\varepsilon \quad (1)$$

η is the electrode overpotential, $\eta = E - E_0$, E_0 the standard redox potential, and E the electrode potential. e (<0) is the electronic charge. The Fermi level is taken as zero. Positive $e\eta$ gives a negative reaction Gibbs free energy. The electronic energy levels in the electrode, ε, are counted from the Fermi energy ε_F. $f(\varepsilon)$ is the Fermi function, $\rho(\varepsilon)$ the level density, and $W(\varepsilon;\eta)$ the transition probability per unit time (rate constant) at the overpotential η involving the level ε. The rate constant holds further the activation free energy with the reorganization free energy, E_r, and the electron exchange factor $T(\varepsilon)$. k_B is Boltzmann's constant, T is temperature, and $2\pi\hbar$ Planck's constant. Equation 1 implies that we consider the diabatic ("nonadiabatic") limit of weak interaction between the molecule and the electrode, warranted by the long ET distance. As implied by $T(\varepsilon) \to T(\varepsilon_F)$, levels around the Fermi level dominate over broad overpotential ranges when $|e\eta| < E_r$.

Scaling all energy quantities with respect to $k_B T$,

$$E = \frac{E_r}{k_B T},\ x = \frac{\varepsilon}{k_B T},\ \text{and}\ \zeta = \frac{e\eta}{k_B T} \quad (2)$$

and introducing the electronic broadening of the molecular redox level, we obtain

$$\Delta_{el,mol} = \pi[T(\varepsilon_F)]^2\rho(\varepsilon_F);\ \Delta_{el,mol}^{norm} = \frac{\Delta_{el,mol}}{k_B T}i = \frac{e}{\hbar}\sqrt{\frac{1}{\pi E}}k_B T\left\{\Delta_{el,mol}^{norm}\int_{-\infty}^{\infty}\frac{1}{1+e^x}\exp\left[-\frac{(E-\zeta-x)^2}{4E}\right]\mathrm{d}x\right\} \quad (3)$$

Equation 3 is convenient for numerical consideration. We can also represent eq 3 as

$$i = e\frac{\omega_{eff}}{2\pi}\kappa_{eff}\left\{\int_{-\infty}^{\infty}\frac{1}{1+e^x}\exp\left[-\frac{(E-\zeta-x)^2}{4E}\right]\mathrm{d}x\right\};\quad \kappa_{eff} = \Delta_{elec,mol}^{norm}\sqrt{\frac{4\pi^2}{E(\hbar\omega_{eff}^{norm})^2}} \ll 1 \quad (4)$$

where ω_{eff} is the effective vibrational frequency of all the classical nuclear modes reorganized and

$$\hbar\omega_{eff}^{norm} = \frac{\hbar\omega_{eff}}{k_B T} \quad (5)$$

The adiabatic limit takes over when $[T(\varepsilon_F)]^2\rho(\varepsilon_F)k_B T \approx 10^{-4}$ eV^2. The dominating effect of the orbital overlap is then to decrease the ET activation barrier and in this way accelerate the reaction, most conveniently further addressed using the Anderson−Newns formalism.[59]

2.2. Coherence and Incoherence in (Bio)-electrochemical NP-Mediated Two-Step ET. Equations 1−5 also offer a frame for the catalytic mechanism, either as a coherent transition between a given electrode electronic level and the molecular redox level, via intermediate AuC levels, or as two sequential single-ET processes.

2.2.1. Coherent Two-Step Electrochemical ET: AuC-Mediated Superexchange. Equation 1 applies again but now in the following form:[60−62]

$$i = \frac{e}{\pi\hbar}\int_{-\infty}^{\infty}\mathrm{d}\varepsilon_{elec}\int_{-\infty}^{\infty}\mathrm{d}\varepsilon_{part}f(\varepsilon_{elec})[1-f(\varepsilon_{part})]f(\varepsilon_{part})\times\sqrt{\frac{\pi}{E_r k_B T}}\frac{\Delta_{elec,part}\Delta_{part,mol}}{(\varepsilon_{elec}-\varepsilon_{part})^2+(\Delta_{elec,part}+\Delta_{part,mol})^2}\exp\left\{-\frac{[E_r - e\eta - \varepsilon_{elec}]^2}{4E_r k_B T}\right\} \quad (6)$$

ε_{elec} and ε_{part} are the electronic energies in the electrode and the AuC, respectively. $\Delta_{elec,part}$ and $\Delta_{part,mol}$ are the broadening of the AuC energies by coupling to the electrode and the molecular level, respectively. A Lorentzian instead of a weakly varying density of states emerges supported by DFT calculations, Section 3. We have assumed that the potential drop between electrode and molecule is entirely in the AuC/solution step. This constraint can be relaxed once the real potential distribution is known. Coupling is thus purely electronic, denoted as "superexchange".

There are now *two* Fermi functions. One gives the probability that there is an available electron in the electrode; the other one, that there is a vacant level on the particle. The reverse would apply to hole transfer. Similar views were introduced earlier.[39,40,46] The denominator gives an energy resonance. Broadening factors in the denominator represent lifetime processes in which the intermediate AuC-localized electron can participate. We identify these as ET between the AuC and the electrode or the redox molecule, but other processes could prevail. The broadening factors in the denominator and in the numerator may therefore not be the same.

We can also recast eq 6 in dimensionless form:

$$i = \frac{e}{\hbar}k_B T\sqrt{\frac{1}{\pi E}}\left\{\int_{-\infty}^{\infty}\mathrm{d}x\int_{-\infty}^{\infty}\mathrm{d}y\frac{1}{1+e^x}\frac{e^y}{(1+e^y)^2}\times\frac{\Delta_{elec,part}^{norm}\Delta_{part,mol}^{norm}}{(x-y)^2+(\Delta_{elec,part}^{norm}+\Delta_{part,mol}^{norm})^2}\exp\left[-\frac{(E-\zeta-x)^2}{4E}\right]\right\}\quad x = \frac{\varepsilon_{elec}}{k_B T};\ y = \frac{\varepsilon_{part}}{k_B T} \quad (7)$$

The curly brackets on the right-hand sides of eqs 4 and 7 can thus be directly compared. We consider next this difference in the competition of coherent two-step ET with single-step ET.

2.2.2. Single-Step and Coherent Two-Step Electrochemical ET: A Simple Comparison. We first provide a "coarse-grained" comparison between single- and coherent two-step ET, applying the following crude forms:

$$\Delta_{elec,mol}^{norm} = \Delta_{elec,mol}^{norm,0}\exp(-\beta L_1) \quad (8)$$

where L_1 is the distance between the electrode and the redox molecule (≈ 10−15 Å, Figure 1). β is the electronic decay factor, and $\Delta_{elec,mol}^{norm,0}$ is a constant. The coherent two-step ET form is

$$\Delta_{part}^{norm} \approx \Delta_{elect,mol}^{norm,0}\exp(-\beta_1 L_1)\times\exp(-\beta_2 L_2) \quad (9)$$

where L_1 and L_2 are the electrode/AuC and the AuC/redox molecule distances, respectively, and β_1 and β_2 are the corresponding decay factors. We assign the same value

https://dx.doi.org/10.1021/jacs.9b09362
J. Am. Chem. Soc. XXXX, XXX, XXX−XXX

$\Delta^{\mathrm{norm},0}$ to the two steps. We can then give the AuC-induced current amplification in the form

$$\frac{\Delta^{\mathrm{norm}}_{\mathrm{part}}}{\Delta^{\mathrm{norm}}_{\mathrm{el,mol}}} = \exp[(\beta - \beta_1)L_1 + (\beta - \beta_2)L_2] \tag{10}$$

We addressed ET between a metal electrode and a spherical metallic nanocluster (i.e., β_1) using the free electron approach of Gao and Marcus[63] (discussed in the SI), giving $\beta_1 \approx 1$ Å^{-1} and depending only weakly on the cluster radius. Most reported β-values for direct ET via alkanethiol molecular linkers are also around $\beta \approx 1$ Å^{-1},[64,65] which accords with our calculations, Section 3.2. Using these findings we can reduce eq 10 to

$$\frac{\Delta^{\mathrm{norm}}_{\mathrm{part}}}{\Delta^{\mathrm{norm}}_{\mathrm{el,mol}}} \approx \exp[(\beta - \beta_1) - \beta_2)L_2] \approx \exp(-\beta_2 L_2) \ll 1 \tag{11}$$

suggesting that coherent two-step ET is not competitive due to the longer ET distance. This is not compensated by favorable AuC electronic "spillover" (smaller β-values) compared with a planar surface. Neither is it compensated by the Lorentzian resonance (eq 7, Figure S1). The Lorentzian energy denominator counteracts the distance decay with a resonance feature when the electrode/AuC energy gap gets small or vanishes, reflected in a maximum at $\zeta \approx -E$, or $|e\eta| \approx E_r$ (eqs 6 and 7), Section 3.3, shifted from "ordinary" voltammetric peaks at $\eta \approx 0$. However, if ET between the AuC and the electrode or the molecule causes the broadening, the energy resonance is not competitive (Figure S1) and other lifetime mechanisms would be needed. Raman scattering is a two-step optical analogue where electronic processes separate from the optical excitation and emission controls the broadening. Refs 66 and 67 offer discussions of these points. A cautious conclusion is then that coherent two-step current enhancement is unlikely, unless ET broadening rooted in size-dependent electronic density expansion exceeds the expansion from a planar surface *and* intermediate state lifetime broadening is significantly weaker. Our analysis in Section 3 shows that such effects are not likely.

2.2.3. Incoherent Two-Step Electrochemical ET. "Incoherent" two-step interfacial ET via the AuC implies vibrational relaxation in the intermediate electronic state, with an excess electron or hole distributed over a manifold of electronic energy levels. The starting point is the steady state excess electron (electron or hole) transport between the electrode and the molecule via the AuC, eq 12. Formally similar schemes were used in related contexts of consecutive electrochemical ET processes of multicenter Cu enzymes[68,69] and of *in situ* scanning tunneling microscopy of redox molecules:[70]

$$\text{Electrode} \underset{\overleftarrow{k}_1}{\overset{\vec{k}_1}{\rightleftarrows}} \text{AuC} \underset{\overleftarrow{k}_2}{\overset{\vec{k}_2}{\rightleftarrows}} \text{molecule} \tag{12}$$

The rate constants $\vec{k}_1$ and $\vec{k}_2$ describe ET from the metal surface to the AuC and from the AuC to the molecule, respectively, $\overleftarrow{k}_1$ and $\overleftarrow{k}_2$ denote the reverse ET processes from the AuC to the metal and from the molecule to the AuC, respectively.

Following the scheme in the Supporting Information (SI), Section S12, the following rate constant form can be derived

$$k = \frac{\vec{k}_1\vec{k}_2 - \overleftarrow{k}_1\overleftarrow{k}_2}{\vec{k}_1 + \vec{k}_2 + \overleftarrow{k}_1 + \overleftarrow{k}_2} \tag{13}$$

We can take $\vec{k}_1, \vec{k}_2 \gg \overleftarrow{k}_1, \overleftarrow{k}_2$, reducing eq 13 to

$$k = \frac{\vec{k}_1\vec{k}_2}{\vec{k}_1 + \vec{k}_2}, \text{ or } i^c = e\frac{\vec{k}_1\vec{k}_2}{\vec{k}_1 + \vec{k}_2} \approx e\overrightarrow{k_2} \tag{14}$$

The two-step current thus takes the same form as for single ET, now between the AuC and the redox molecule. As the voltammograms of the AuC-catalyzed processes follow those of direct ET, the electrochemical potential of the AuC must follow that of the working electrode.

$\vec{k}_2$ represents ET between the AuC and the redox molecule. The rate constant form is analogous to eq 4, the main difference being that the coupling factor, $\Delta^{\mathrm{norm}}_{\mathrm{elec,mol}} = \Delta_{\mathrm{elec,mol}}/k_BT$ involving the electrode and the molecule is replaced by the coupling between the AuC and the molecule, $\Delta^{\mathrm{norm}}_{\mathrm{part,mol}} = \Delta_{\mathrm{part,mol}}/k_BT$. Comparing direct and AuC-mediated ET now over the same distance, we can write

$$\frac{\Delta^{\mathrm{norm}}_{\mathrm{part}}}{\Delta^{\mathrm{norm}}_{\mathrm{elec,mol}}} = \exp[(\beta - \beta_2)L_2)] \tag{15}$$

Taking again the two contact lengths to be the same, $L_1 = L_2 = L$, the enhancement condition is then the much milder $\beta_2 < \beta$. The largest cluster Au_{147}, closest in size to "real" electrocatalytic AuCs, and the Au_{19} ridge site (at short distances) come closest to being competitive, but different surface sites show high selectivity, Section 3. It therefore seems that current amplification by incoherent two-step ET could be a competitive single-AuC catalytic ET mechanism for given AuC sizes, surface sites, and ET distances. As we shall see, this overarching conclusion carries over for a superexchange AuC/Fc^+ ET mechanism via an adsorbed alkyl thiyl "tail".

3. DFT OF THE ELECTRONIC STRUCTURE AND ELECTRON EXCHANGE OF MOLECULAR SCALE Au CLUSTERS

In Section 2 we provided a simplified view of AuC-mediated diabatic electrochemical ET and identified electronic requirements for AuC electronic density "spillover" to prevail over direct ET. In this Section we introduce a more rigorous approach to the AuC electronic structure and the transmission coefficient for ET between variable-size AuCs and the Fc/Fc^+ probe molecule. As a reference we consider first how far a much simpler model, the spherical free electron model, can account for the transmission coefficient. We consider details of this model and of the other major ET parameter, the solvent reorganization free energy E_r, in the SI.

3.1. Free Electron Model with Finite Energy Boundaries. The free electron model with finite energy boundaries (FEMFB) describes a metallic NP or nanocluster as a spherical box with radius a and a step-like potential:[71]

$$U(r) = \begin{cases} W_e, \text{ if } r \geq a \\ 0, \text{ if } r \leq a \end{cases} \tag{16}$$

W_e is the electronic work function.[52,53] We analyze this model in the SI, with representative results given in Table S1. We calculated further the electron exchange factor, $V_{\mathrm{if}}(\varepsilon_F) \approx VS_{\mathrm{part,mol}}$ as a function of the reactant−NP surface distance x for two different radii. $S_{\mathrm{part,mol}}$ is the overlap integral and V was

https://dx.doi.org/10.1021/jacs.9b09362
J. Am. Chem. Soc. XXXX, XXX, XXX−XXX

taken as the potential energy of the electron in the Coulombic potential of the molecule at the point of maximum overlap x^{max}, $V = -e^2/x_{max}$. The overlap integrals, $S_{part,mol} = \langle\psi_{part}(r)\psi_{mol}(r)\rangle \approx \exp(-\beta_{part}L)$, were combined with $\psi_{mol}(r)$ as a 1s hydrogen atom-like wave function. $V_{if}^2(x)$ is shown in Figure 2. The slopes were estimated as 2.26−2.36 Å^{-1}.

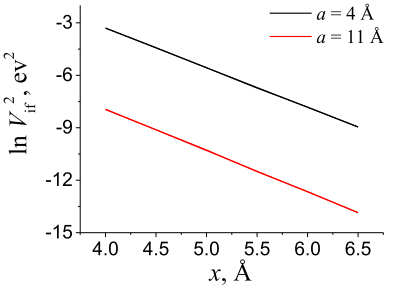

Figure 2. Square of the resonance integral $V_{if} = V\langle\psi_{part}(r)\,\psi_{mol}(r)\rangle$ vs the separation between the molecular reactant and the FEMFB surface. Two different radii are considered.

The FEMFB analysis suggests that the electron exchange factor varies exponentially with distance, representative of the transmission coefficient for electron exchange between the free electron object and a hydrogen-like reactant. The distance decay factor of the wave function follows roughly the inverse particle work function; that is, the smaller the particle, the larger the work function.[52] The distance variation solely by the exponential decay factors thus gives a smaller overlap factor the smaller the particle. This effect is overcompensated by the normalization factor, B in eq S2, which scales with the particle size. As a result, the overlap integrals *decrease*—notably—with increasing size, and the rate constant is expected to be smallest for a bulk surface. The FEMFB thus offers indications that ET between a free electron object and a molecular reactant is more efficient that between a bulk surface and a molecular reactant.

3.2. Au Cluster Models and Electronic Densities of States of Au_{19}–Au_{147} Au Clusters. We explored the electronic structures, densities of state (DOS), and the transmission coefficients of Au_{13}, Au_{19}, Au_{55}, Au_{79}, and Au_{147} AuCs at the DFT level based on the hybrid functional b3pw91 as implemented in the Gaussian 16 program suite.[72] A split-valence basis set of double-ζ (DZ) quality was employed to

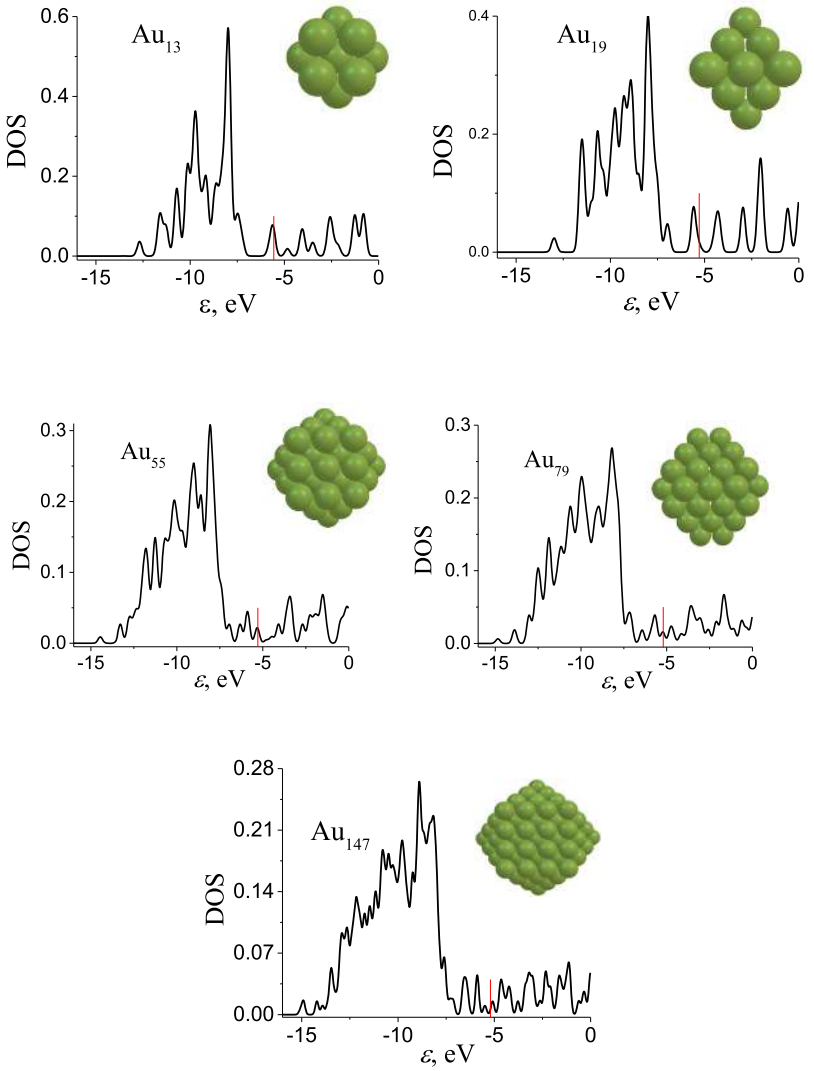

Figure 3. DOS (normalized per single electron) calculated for Au_{13}, Au_{19}, Au_{55}, Au_{79}, and Au_{147} AuCs. The Fermi level (HOMO energy) is noted by vertical red lines.

https://dx.doi.org/10.1021/jacs.9b09362
J. Am. Chem. Soc. XXXX, XXX, XXX−XXX

describe the valence electrons of the Au and Fe atoms. Inner electrons were included in the relativistic core potential (LanL2) of Hay and Wadt.[73] The Dunning−Huzinaga valence basis set (D95V) was used to describe the electrons of C and H atoms.[72] The open-shell systems were treated in an unrestricted formalism. The geometry of the gold clusters was fixed according to the crystallographic fcc structure. The electronic AuC density of states was calculated using the Gaussian software.[72] The transmission coefficients were calculated using an approach developed previously[58,59] (Section S5 in the SI). Two different orientations of the Fc molecule (vertical and horizontal) were considered (Section S6 in the SI).

Figure 3 gives a visual impression of the AuCs most relevant to electrocatalysis. Au_{13} (with just a single Au atomic shell around a central Au atom) is the smallest Au single crystal. Au_{79} (1.3 nm) and Au_{147} (1.7 nm) are getting closer to "real" AuC catalysts, while Au_{55} is an intermediate "magic size" with two coordinating Au-atom shells. Fcc structures were built and used, and transmission coefficients for all three low-index surfaces, Au(111), Au(100), and Au(110), as well as for vertex and ridge structural elements were calculated. The Au_{13}, Au_{19}, Au_{55}, Au_{79}, and Au_{147} DOSs are also shown. Some other characteristics are given in Table 1.

Table 1. HOMO (Highest Occupied Molecular Orbital) Energies (ε_{HOMO}) of the Au_{19}, Au_{55}, Au_{79}, and Au_{147} Clusters and Radii (r_{eff}) of Approximately Spherical Cluster Representations

	Au_{13}	Au_{19}	Au_{55}	Au_{79}	Au_{147}
ε_{HOMO}, eV	−5.56	−5.28	−5.29	−5.20	−5.05
r_{eff}, Å	2.9	4.1	5.8	6.1	8.6

The Au_{13}, Au_{19}, Au_{55}, Au_{79}, and Au_{147} DOSs reflect clearly a discrete electronic energy spectrum. The energy spacing is not entirely equidistant. Although a frame for single-electron/hole charging (SET), the discrete energy spectrum is therefore not solely caused by simple capacitive SET.[28−32] The DOS patterns display both major peaks and subpeaks with significantly larger peak values below than above the Fermi level (HOMO). The computed peak separations are still a useful SET frame in both interfacial electrochemical ET and *in situ* STM as observed.[28−34]

3.3. Current−Overpotential Relations of Variable-Size Molecular Scale Au Nanoclusters. Figure 4 shows j/η correlations for ET between Au_{13}, Au_{19}, Au_{55}, Au_{79}, and Au_{147} clusters and Fc^+, the transmission coefficient here taken as unity. Results for a planar surface are also shown. The reorganization (free) energy E_r was calculated using simple dielectric models (see SI and Table S1). A constant density of states ($1/U_0$, where U_0 is the band conductivity bottom, ca. 11 eV[74]) was used for the planar metal electrode. As the DOS is normalized per single electron, the effective number of electrons participating can be included in the transmission coefficient.

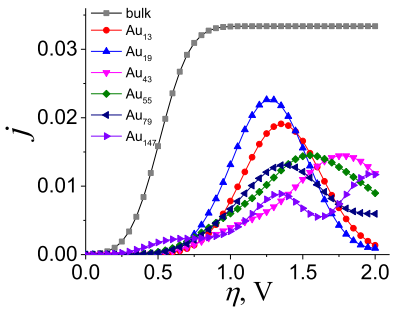

Figure 4. Current/overpotential dependence for ET between Fc^+/Fc and three different AuCs as well as for a bulk metal with constant DOS. The electronic transmission coefficients are taken as unity, but the DOSs are explicitly incorporated.

The correlation for the planar Au(111) surface is approximately exponential at small overpotential followed by activationless behavior as $|e\eta| \geq E_r$, as determined by the continuous electronic energy spectrum with weakly energy dependent DOS.[39,40] AuCs with discrete electronic spectra show instead a resonance feature, corresponding to eq 6 and Figure S1 and conceptually related to the inverted free energy range of optical[75−78] and thermal electronic processes.[77,79−81] The resonance is sharp for Au_{19} but broadens and is shifted as the AuC size and level density increase.

Viewed from another angle, the resonance appears at high overpotentials, $|e\eta| \geq E_r$, where the discrete AuC electronic levels, Figure 4, successively prevail, resembling "chemical spectroscopy" of ET reactions[80,81] introduced early but substantiated only recently.[82] The resonance finally displays a nonmonotonic AuC size dependence, assigned to specific electronic AuC features.

3.4. Electronic Transmission Coefficients for ET between the Au Clusters and Fc/Fc^+. *3.4.1. "Naked" Au Clusters.* The electronic transmission coefficient, κ_{el}, and the solvent reorganization free energy, E_r, are the two core parameters that control the ET between the AuCs or a planar electrode surface and the Fc/Fc^+ molecule. We discuss here the DFT-computed transmission coefficients. Details of calculations are given elsewhere.[58,59] We first address the electronic structure of Fc/Fc^+ and the AuCs considering two acceptor molecular orbitals and two Fc^+ orientations relative to the AuC surface sites. The sandwich ligand orientation perpendicular to the AuC faces or ridge and vertex structures was found to prevail by far and is what is addressed below, but our preliminary calculations show that alkanethiols S-$(CH_2)_n$-CH_3 (n = 6, 10) are adsorbed preferentially on bridge or hollow sites, with significant tilting flexibility, which in turn leads to a variety of orientations of the Fc molecule. The structures discussed below and in the Supporting Information are the equilibrium structures. E_r was found to depend only weakly on the cluster size, cf. the SI. The Au−Fe distances range from 4 to 8 Å. The results are less reliable for larger separations due to instability of the Kohn−Sham equations and the need to include Au basis polarization functions.

Figure 5 shows the κ_{el} distance variation for four AuCs. The surface sites are those that give maximum orbital overlap. The distances are those between the Fe center in Fc^+ and the AuC surface. The same distances can therefore be compared for different size AuCs. Both the absolute values and the distance variation depend on the specific AuC surface structural element, faces (111), (100), vertex, and ridge, Figure 6. Approximately exponential dependence emerges for x(Au−Fe) larger than about 5 Å with a tendency toward distance independence at small distances, reflecting the transition from strongly diabatic to adiabatic ET. The (111) and ridge sites of Au_{147} seem to be exceptions but would most likely show the same tendency at shorter distances.

https://dx.doi.org/10.1021/jacs.9b09362
J. Am. Chem. Soc. XXXX, XXX, XXX−XXX

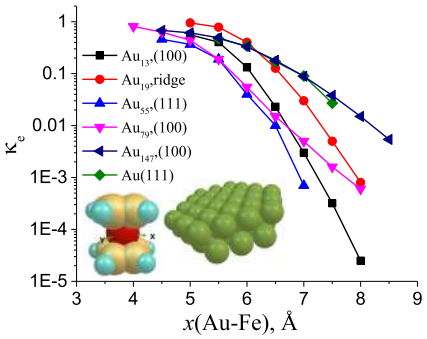

Figure 5. Electronic transmission coefficient (κ_e) vs Au−Fe separation for ET between solute Fc^+/Fc and the prevailing surface sites of five different-size AuCs, as well as the planar Au(111) surface. A vertical Fc^+ orientation with the cyclopentadienyl rings perpendicular to the Au facets and surface edge sites (shown) gives the largest contribution. Inset: Space-filling model of the Fc core and a two-layer $Au_{54}(27 + 27)$ cluster that mimics the Au(111) surface[58] (not drawn to scale).

κ_{el} of the dominating surface ridge channel of the smallest, Au_{19}, cluster exceeds κ_{el} of both the smaller, Au_{13}, and the larger, Au_{55} and Au_{79}, clusters by a factor of 5 or so at large Au−Fe distances and crosses over from about 8 Å for Au_{79} but not for Au_{55}. κ_{el} for Au_{19} exceeds that of both Au_{147} and the planar surface at small distances and crosses over around 6 Å.

The decay factors β_2 are summarized in Table 2. β_2 is largest for Au_{13}, 3.9−4.3 $Å^{-1}$. With the exception of the Au_{55} face

Table 2. Slope Values (β_2, $Å^{-1}$) Calculated for Different AuCs and Surface Sites

	vertex	ridge	face (111)	face (100)
Au_{13}	3.85		4.3	4.3
Au_{19}	2.6	3.1	1.77	
Au_{43}	1.68		1.68	
Au_{55}	1.74	2.05	3.6	
Au_{79}	1.7	1.32		0.98
Au_{147}		1.86	1.71	1.

(111) site (3.6 $Å^{-1}$) β_2 for the larger AuCs is much smaller, clearly tending to decrease with increasing AuC size. Some values compare with the FEMFB values (2.3−2.4 $Å^{-1}$, Section 3.1). The distance dependence with $\beta \approx 1$ $Å^{-1}$ for a planar Au(111) surface[58] is also shown. β_2 is a measure of the electronic "spillover". Only the largest AuCs, Au_{79} and Au_{147}, compete with planar Au(111) in this respect. In all the other cases the spillover contracts compared with the planar surface, suggesting that AuCs above a certain size are needed for catalysis, but our computational limitations are prohibitive for AuCs larger than Au_{147} to see if more extensive spillover arises for AuCs closer to the size in real catalysis. Further, the values

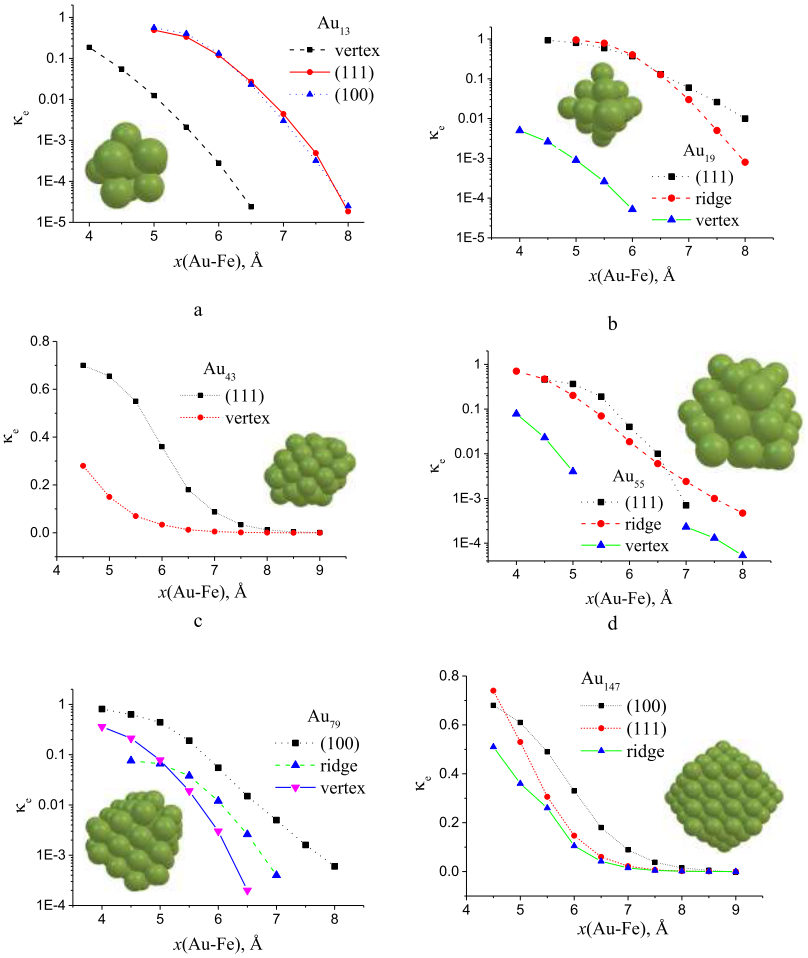

Figure 6. Electronic transmission coefficient vs distance calculated for the different AuCs and surface sites. The Fe atom is projected onto the AuC (111) and (100) faces, vertex, and ridge. Inset: Space-filling atomic models of the AuCs.

https://dx.doi.org/10.1021/jacs.9b09362
J. Am. Chem. Soc. XXXX, XXX, XXX−XXX

of κ_{el} for the Au_{19} cluster ridge site and for the Au_{79} and Au_{147} face (100) site are larger than for planar Au(111), at distances less than 5−6 Å for Au_{19} and Au_{79}, but only in the more strongly diabatic range, >7.5 Å for Au_{147}. The crossover behavior resembles recent observations[83] on ET across (111) faces and monatomic rods for several d-metals. Six angstroms is therefore a kind of "turnover" point.[84] The origin of this effect is rooted in subtle electronic density features of the Me(111) surface and the cluster or nanorod.

The sensitivity of the κ_{el}/x(Au−Fe) distance correlation to the AuC surface structure is illustrated further in Figure 6 for the prevailing (111) and (100) faces, vertex (a-top), and ridge sites. In general the face and ridge sites give significantly larger orbital overlap than the vertex site.

3.4.2. Effects of AuC Thiyl Adsorption. We considered so far direct ET from a AuNC to Fc^+. AuNP catalysis of simple ET processes mostly involves thiol-coated AuNPs. We therefore next analyze bridge-assisted ET (BAET) via an adsorbed alkanethiyl molecule. We addressed first thiol adsorption on the electronic structure of the Au_{55} cluster solely with two sulfur atoms adsorbed in bridge position mimicking the Au−S surface bonding. Although there is some "mixing" of the S orbitals in the frontier orbitals of the $Au_{55}\cdot 2S_{ads}$ cluster, the orbitals remain basically "metallic" and well delocalized over the entire AuC, Figure S7. The effect of the S atoms on the molecule−AuC orbital overlap is thus small, especially for large AuCs, with little effect on the transmission coefficients. Surface-enhanced Raman spectroscopy (SERS) can provide other insight into the nature of the Au−S electronic states involved.[51] The effect of the thiol tail on the acceptor orbitals of the redox molecule was also found to be small, as seen in the S-$(CH_2)_6$-Fc molecular unit, Figure S8. This observation justifies our model employed to address direct ET.

Assuming single-band electronics, the resonance splitting ΔE_e for BAET via a single alkanethiol molecular bridge can be written as[39,85−87]

$$\frac{\Delta E_e}{2} \approx \frac{V_{DB}V_{BA}}{\Delta U^*}\left(\frac{\beta}{E-\alpha}\right)^n \quad (17)$$

V_{DB} and V_{BA} are the electronic factors describing the orbital overlap between the donor and S-CH_2− bridge and the acceptor and −CH_2−CH_3 bridge, respectively. The energy gap ΔU^* is shown in Figure S4, β is a coupling parameter for interaction between neighboring −CH_2-CH_2− bridge orbitals, α is the energy of an individual bridge orbital, E is the energy of the electron to be transferred (in the following we assumed that $E \approx \Delta U^*$), and n is the number of −CH_2-CH_2− bridge units.

The slope of the dependence of the electronic transmission coefficient on distance is defined in this case by the $\left(\frac{\beta}{E-\alpha}\right)^n$ term and is about 1.1 $Å^{-1}$, which is close to experimental observations.[87] This formalism is employed in the present work to investigate BAET for the Au(111)/S-$(CH_2)_5$-CH_3/RTIL (room temperature ionic liquid) interface. The choice of this system is warranted by reported MD simulation data,[88] especially the potential of mean force (Gibbs energy profile), which enables determining the distance of closest approach of Fc^+ to the −CH_2-CH_3 tail. This distance is in fact large, i.e., 1.5 nm or so, implying that the ET process involves tunneling through an extended region of solvent in addition to the thiyl linker. No such MD data are presently available for aqueous electrolyte solution or for electrostatically charged probe molecules, but with the hydrophobic nature of the probe Fc/Fc^+ molecule in the present study, we shall assume that the IL data carry over to aqueous solution, at least qualitatively. The model system used is shown in Figure S5 (left) and mimics a target S-$(CH_2)_6$-Fc molecule. The Au(111) surface was again modeled by the Au_{54} cluster. V_{DB} and V_{BA} were calculated similarly to the scheme for direct ET. We considered an excited triplet S-$(CH_2)_5$-CH_3^- anion configuration (singlet ground state) as a virtual state. This configuration provides efficient orbital overlap for both Au(111)-S-CH_2− and −CH_2-CH_3-Fc (Figure S5, right). The solvent reorganization free energy was estimated using the model of Liu and Newton.[89] β and α were taken from extended Hückel parametrization (2.3 and 11.3 eV, respectively). Some results shown in Figure S6 are strongly indicative of significantly diabatic ET. In the region of closest approach (∼15 Å) BAET is slightly faster than direct ET (by a factor of ∼2) but from $x \geq 16$ Å direct ET is favored. Direct and BAET are therefore at least competitive.

We extended this analysis to variable-size AuCs. Our analysis discloses preferential S-$(CH_2)_n$-CH_3 (n = 6, 10) alkanethiol adsorption on bridge or hollow sites with significant tilting flexibility, opening for a variety of orientations of the Fe molecule and of BAET and catalytic patterns depending on AuC size and surface site. The data and conclusions below rest on equilibrium structures of the AuC adsorbed −S-$(CH_2)_6$-Fc unit. We note some results, although they are preliminary in view of the diversity of ET patterns and the fact that at this stage only a single 6C alkanethiol linker unit rather than a whole alkanethol monolayer could be addressed.

First, V_{DB} is the only quantity sensitive to the AuC electronic structure, eq 16. From our calculations, the V_{DB} values for small AuCs (Au_{13}, Au_{19}) notably exceed those for larger AuCs, and V_{DB} decreases as (111) > (100) ≈ edge for Au_{79}. V_{DB} and V_{BA} are also practically independent of the alkanethiol (S-$(CH_2)_n$-CH_3 length, n = 3−13). Second, the distance dependence of the transmission coefficient in the region of closest approach (Figure S6) suggests that BAET competes with direct ET up to about the distance of closest approach, but direct ET prevails at larger separations. A cautious conclusion is then that the calculated rate constant enhancement for BAET between a AuC and Fc/Fc^+ via adsorbed alkanethiyl/solution compared to direct ET is close to the 2- to 3-fold catalytic ET enhancement for "naked" AuCs. AuC-catalyzed and direct ET are therefore at least competitive in both cases.

4. DISCUSSION AND SOME NOTES OF CONCLUSION

Molecular scale (2−5 nm) nanoclusters of Au and other (noble) metals are catalysts of simple electrochemical ET processes that involve transition metal complexes, quinones, metalloproteins such as cyt *c* and azurin, and redox enzymes.[15−17] Rationales as to the origins of the up to 20-fold AuC-triggered rate increase have been forwarded.[6,7,10,11,14,18,49] In this report, using theoretical methods, we have explored whether the electronic properties of a single molecular-size AuC offers clues to the catalysis of simple electrochemical ET processes.

We focused on ET between a probe molecule, here Fc^+/Fc, and a planar model Au(111)-electrode surface, via a single variable-size molecular scale AuC. The diabatic limit is used for both the molecule/AuC and the AuC/Au(111) contact. Focus is on the AuC density of electronic states and the transmission

https://dx.doi.org/10.1021/jacs.9b09362
J. Am. Chem. Soc. XXXX, XXX, XXX−XXX

coefficient between a single AuC and Fc/Fc^+. We considered two mechanisms. One is "superexchange", in which ET between the electrode and the molecule proceeds in a single step coupled purely electronically via the AuC. The second mechanism is sequential two-step ET between the AuC and the molecule and between the AuC and the electrode. The excess electron or hole is here physically located on the AuC. We considered first general requirements regarding electronic factors needed for competitive two-step AuC-mediated ET vs direct single-step ET. With two electronic factors, superexchange is electronically significantly more demanding than sequential two-step ET, as the latter formally reduces to the single-ET form with only a single electronic factor. Sequential two-step ET was therefore in focus in our further analysis.

As a first illustration, we used a free electron model with finite barriers (FEMFB) combined with a hydrogen atom-like molecular probe. Although crude, this model shows clear size-dependent transmission coefficients with faster ET the smaller the free-electron particle entity. This is opposite of expectations based solely on size-dependent work functions,[52,53] Table S1. The FEMFB analysis was followed by DFT analysis of "naked" Au_{13} to Au_{147} AuCs. We could not address larger AuCs closer to the real catalytic AuC size range,[6−11,13,14] but DFT and Au_{19}−Au_{147} nanocrystal models enable precise mapping of the AuC DOS and transmission coefficients including the three low-index AuC faces, as well as ridge and vertex AuC surface structural elements.

The transmission coefficients, κ_{el}, display a transition between weak distance dependence at small distances, $\lesssim$5−6 Å, close to the adiabatic limit and exponential decay at larger distances in the diabatic limit, Figure 5. The decay factors depend strongly on the AuC size and on specific surface structural elements (ridge, vertex, faces), ranging from 1.0 $Å^{-1}$ to >4 $Å^{-1}$, and reflect both potential catalytic effects and electronic density "spillover". Roughly, the larger the AuC in the Au_{13}−Au_{147} range, the stronger the "spillover", and therefore the stronger the catalysis. κ_{el} is also exceedingly sensitive to the AuC surface structural elements, Figure 6, and the most efficient sites differ as the AuC size increases. As the only AuCs and structural surface sites, Au_{19} (ridge) and Au_{79} and Au_{147} (face 100) are competitive with a planar Au(111) surface. The competitiveness is restricted to a 2−3-fold rate increase and does not reach the order of magnitude observed. The rate enhancement also exhibits intriguing crossing over distance dependence from about 6 Å for Au_{19}, Au_{79}, and Au_{147}. Extension to larger AuCs might disclose more pronounced spillover and catalysis.

"Real" AuC-catalyzed ET processes involve other perspectives. For reasons of computational challenge we first addressed "naked" AuCs, with the outcomes noted, as opposed to AuCs protected by a thiol (SAM).[6−11,13,14] Thiyl-based SAMs affect the transmission coefficients by opening thiyl-based superexchange channels. We could not compute the effects of a whole thiyl SAM, but to illuminate the thiyl effects, we addressed in several stages the electronic effects (BAET) of a single adsorbed thiyl molecule. We addressed first a $Au_{55}C$ with two bridge-adsorbed S atoms (Figure S7a), then a S-$(CH_2)_6$-Fc molecular entity (Figure S9), and finally the electronic transmission coefficient in BAET of the whole AuC/thiol/Fc entity. There is some "mixing" of the S orbitals in the frontier orbitals of the $Au_{55}{\cdot}2S_{ads}$ cluster, but the orbitals remain largely "metallic" and delocalized over the AuC, Figure S7. The direct effect of the S atoms on the molecule−AuC orbital overlap is thus small, especially for large AuCs, with little effect on the transmission coefficients when assuming direct ET. Second, although no MD simulations of the distance of closest approach of Fc^+ to the A(111)/SAM (alkanethiols) interface are available for aqueous electrolyte solution, such data for Fc in ionic liquids[88] suggest that this distance could be nearly 15 Å (with respect to the Au surface). The calculated distance-dependent transmission coefficient, Figure S6, is then indicative that BAET and direct ET are competitive at the distance of closest approach. Different conformations of an alkanethiol linker might enhance the role of BAET. A cautious conclusion is, then, that the 2-to-3-fold catalytic rate constant enhancement computed for ET of the "naked" AuCs may carry over to BAET via the alkanethiyl/solution matter. Further work along these lines is in progress.

The other core parameter, the reorganization free energy, E_r, is addressed in the SI. E_r varies by about 0.2 eV in the AuNP size range from $\leq$1/2 nm to a planar electrode surface, corresponding to an activation free energy variation of 0.05 eV or 7-fold rate constant variation. E_r thus favors large AuNPs or planar surfaces, i.e., opposite of the size effects of the electronic factor. This conclusion is based on the solvent as a structureless, homogeneous dielectric medium. Frequency and spatially dispersive solvent effects as well as local structural features could, however, operate in the inhomogeneous and anisotropic interfacial region between the electrode surface and the bulk solvent,[39,40,90] leading to short-range, weakly size dependent solvent effects with only a minor contribution from the solvent reorganization compared with the purely electronic effects.

A third notion relates to surface charge effects on the transmission coefficient. Excess negative charging causes expansion of the electronic spillover and increased transmission coefficients and excess positive charging to electronic density contraction with decreasing interfacial ET rates. These effects were analyzed for planar jellium surfaces.[54−56,90−92] The effects are small for mercury and gold but much stronger for electronically lighter metals such as silver. This may, however, be different for heavy metals in nanocluster form. Still another outcome relates to the j/η correlation, Figures 4 and S1. As noted, the correlation for a planar macroscopic Au(111) surface is sigmoidal, rooted in the continuous energy spectrum and weakly energy dependent DOS.[39,40] A resonance feature emerges for AuCs with a discrete electronic spectrum, noted to hold conceptual relations to optical[75−78] and thermal[79−81] electronic processes. The resonance is sharpest for the smallest particles and is broadened and shifted as the AuC size increases toward increasing level density.

We can finally compare the single-AuC approach to catalytic ET processes presently introduced with the collective AuC view of Chavalziel and Allongue.[49] Their approach could rationalize rate enhancements based on a view of fluctuationally triggered formation of a two-dimensional surface AuC array from a disordered thiyl-linked AuC layer. As for the single-AuC-based view presently introduced, the role of the molecular linkers between the AuCs is, however, in need of exploration. A cautious overall conclusion is then that single-AuC catalysis of simple electrochemical ET processes between a Au electrode and Fc/Fc^+ via a AuC is likely for "naked" solute AuCs and for BAET via a AuC linked to Fc/Fc^+ through an adsorbed alkanethiyl molecule. The catalytic effects of the most favorable surface sites and distances amount to a 2−3-fold rate increase, notably smaller than observed. The size-

https://dx.doi.org/10.1021/jacs.9b09362
J. Am. Chem. Soc. XXXX, XXX, XXX−XXX

based tendency of Au_{147}, which approaches the size of real AuC catalysts, however, indicates that computations, applied to larger AuCs—and more complete SAMs—might lead to more conspicuous effects.

■ ASSOCIATED CONTENT

Supporting Information

The Supporting Information is available free of charge at https://pubs.acs.org/doi/10.1021/jacs.9b09362.

Superexchange resonance feature; free electron model; electron transfer between a metal electrode and a spherical nanoparticle; solvent reorganization free energy; details of the calculations of the electronic transmission coefficient; electronic structure of the Au cluster with two sulfur atoms adsorbed; two different orientations of the Fc molecule; electronic structure of the S-$(CH_2)_6$-Fc molecule; thiol-promoted superexchange; surface charge and electronic spillover; Cartesian coordinates of the Au NCs used in calculations (PDF)

■ AUTHOR INFORMATION

Corresponding Authors

Renat R. Nazmutdinov − *Kazan National Research Technological University, 420015 Kazan, Republic of Tatarstan, Russian Federation*; Email: nazmutdi@mail.ru

Jens Ulstrup − *Kazan National Research Technological University, 420015 Kazan, Republic of Tatarstan, Russian Federation; Department of Chemistry, Bldg. 207, Technical University of Denmark, DK-2800 Kgs. Lyngby, Denmark;* orcid.org/0000-0002-2601-7906; Email: ju@kemi.dtu.dk

Authors

Shokirbek A. Shermukhamedov − *Kazan National Research Technological University, 420015 Kazan, Republic of Tatarstan, Russian Federation*

Tamara T. Zinkicheva − *Kazan National Research Technological University, 420015 Kazan, Republic of Tatarstan, Russian Federation*

Michael D. Bronshtein − *Kazan National Research Technological University, 420015 Kazan, Republic of Tatarstan, Russian Federation*

Jingdong Zhang − *Department of Chemistry, Bldg. 207, Technical University of Denmark, DK-2800 Kgs. Lyngby, Denmark;* orcid.org/0000-0002-0889-7057

Bingwei Mao − *State Key Laboratory of Physical Chemistry of Solid Surfaces and College of Chemistry and Chemical Engineering, Xiamen University, Xiamen 361005, Fujian, People's Republic of China;* orcid.org/0000-0002-9015-0162

Zhongqun Tian − *State Key Laboratory of Physical Chemistry of Solid Surfaces and College of Chemistry and Chemical Engineering, Xiamen University, Xiamen 361005, Fujian, People's Republic of China;* orcid.org/0000-0002-9775-8189

Jiawei Yan − *State Key Laboratory of Physical Chemistry of Solid Surfaces and College of Chemistry and Chemical Engineering, Xiamen University, Xiamen 361005, Fujian, People's Republic of China;* orcid.org/0000-0002-0045-6169

De-Yin Wu − *State Key Laboratory of Physical Chemistry of Solid Surfaces and College of Chemistry and Chemical Engineering, Xiamen University, Xiamen 361005, Fujian, People's Republic of China;* orcid.org/0000-0001-5260-2861

Complete contact information is available at: https://pubs.acs.org/10.1021/jacs.9b09362

Notes

The authors declare no competing financial interest.

■ ACKNOWLEDGMENTS

Financial support from the RSF (project no. 17-13-01274), the RFBR (project no.17-03-00619a), and The Danish Council for Independent Research for the YDUN project (to J.Z., project no. DFF 4093-00297) is acknowledged.

■ REFERENCES

(1) Daniel, M.; Astruc, D. Gold Nanoparticles: Assembly, Supramolecular Chemistry, Quantum-Size-Related Properties, and Aapplications toward Biology, Catalysis, and Nanotechnology. *Chem. Rev.* **2004**, *104*, 293−346.

(2) Reimers, J. R.; Picconatto, C. A.; Ellenbogen, J. C.; Shashidhar, R., Eds. *Molecular Electronics III*; Ann. N.Y. Acad. Sci., 2003; Vol. *1006*, pp 1−332.

(3) Moth-Poulsen, K.,Ed. *Handbook of Single-Molecule Electronics*; Pan Stanford Publishing: Singapore, 2016.

(4) Xue, Y. Q.; Ratner, M. A. Microscopic Theory of Single-Electron Tunneling through Molecular-Assembled Metallic Nanoparticles. *Phys. Rev. B: Condens. Matter Mater. Phys.* **2003**, *68*, 235410.

(5) Louis, C.; Pluchery, O. *Gold Nanoparticles for Physics, Chemistry and Biology*; Imperial College Press: London, 2012.

(6) Bradbury, C. R.; Zhao, J.; Fermin, D. J. Distance-independence charge-transfer at gold electrodes modified by thiol monolayers and metal nanoparticles. *J. Phys. Chem. C* **2008**, *112*, 10153−10160.

(7) Kissling, G. P.; Miles, D. O.; Fermin, D. J. Electrochemical charge transfer mediated by metal nanoparticles and quantum dots. *Phys. Chem. Chem. Phys.* **2011**, *13*, 21175−21185.

(8) Vargo, M. L.; Gulka, C. P.; Gerig, J. K.; Manieri, C. M.; Dattelbaum, J. D.; Marks, C. B.; Lawrence, N. T.; Trawick, M. L.; Leopold, M. C. Distance Dependence of Electron Transfer Kinetics for Azurin Protein Adsorbed to Monolayer Protected Nanoparticle Film Assemblies. *Langmuir* **2010**, *26*, 560−569.

(9) Caban, K.; Offenhäuser, A.; Mayer, D. Electrochemical Characterization of the Effect of Gold Nanoparticles on the Electron Transfer of Cytochrome *c*. *Phys. Status Solidi A* **2009**, *206*, 489−500.

(10) Razzaq, H.; Qureshi, R.; Schiffrin, D. J. Enhanced Rate of Electron Transfer across Gold Nanoparticle-Anthraquinone Hybrids. *Electrochem. Commun.* **2014**, *39*, 9−11.

(11) Schiffrin, D. J. Current Topics in Physical and Nanoparticle Electrochemistry. *Curr. Opin. in Physical and Nanoelectrochemistry* **2017**, *4*, 112−117.

(12) Gittins, D. I.; Bethell, D.; Schiffrin, D. J.; Nichols, R. J. A Nanometre-Scale Electronic Switch Consisting of a Metal Cluster and Redox-Addressable Groups. *Nature* **2000**, *407*, 67−69.

(13) Jensen, P. S.; Chi, Q.; Grumsen, F. B.; Abad, J. M.; Horsewell, A.; Schiffrin, D. J.; Ulstrup, J. Gold nanoparticle assisted assembly of a heme protein for enhancement of long-range interfacial electron transfer. *J. Phys. Chem. C* **2007**, *111*, 6124−6132.

(14) Jensen, P. S.; Chi, Q.; Zhang, J.; Ulstrup, J. Long-range Electrochemical Electron Transfer of *Pseudomonas Aeruginosa* Azurin-Gold Nanoparticle Hybrid Systems. *J. Phys. Chem. C* **2009**, *113*, 13993−14000.

(15) Dagys, M.; Laurynenas, A.; Ratautas, D.; Kulys, J.; Vidžiūnaitė, R.; Talaikis, M.; Niaura, G.; Marcinkevičienė, L.; Meškys, R.; Shleev, S. Oxygen Electroreduction Catalyzed by Laccase Wured to Gold Nanoparticles via the Trinulcear Copper Cluster. *Energy Environ. Sci.* **2017**, *10*, 498−502.

(16) Zeng, T.; Frasca, S.; Rumschoettel, J.; Koetz, J.; Leimkühler, J.; Wollenberger, U. Role of Conductive Nanoparticles in the Direct Unmediated Bioelectrocatalysis of Immobilized Sulfite Oxidase. *Electroanalysis* **2016**, *10*, 2302−2310.
(17) Kizling, M.; Dzwonek, M.; Więckowska, A.; Bilewicz, R. Size Does Matter − Mediation of Electron Transfer by Gold Clusters in Bioelectrocatalysis. *ChemCatChem* **2018**, *10*, 1988−1992.
(18) Liu, F.; Kamran, K.; Liang, J.-H.; Yan, J.-W.; Wu, D.-Y.; Mao, B.-W.; Jensen, P. S.; Zhang, J.; Ulstrup, J. On the Hopping Efficiency of Nanoparticles in the Electron Transfer across Self-Assembled Monolayers. *ChemPhysChem* **2013**, *14*, 952−957.
(19) Seminario, J. M.; De La Cruz, C. E.; Derosa, P. A. A Theoretical Analysis of Metal-Molecule Contacts. *J. Am. Chem. Soc.* **2001**, *123*, 5616−5617.
(20) Ko, C.-H.; Huang, M.-J.; Fu, M.-D.; Chen, C.-H. Superior Contact for Single-Molecule Contact: Electronic Coupling of Thiolate and Isothiocyanate on Pt, Pd and Au. *J. Am. Chem. Soc.* **2010**, *132*, 756−764.
(21) Šešelj, N.; Engelbrekt, C.; Ding, Y.; Hjuler, H. A.; Ulstrup, J.; Zhang, J. Tailored Electron Transfer Pathways in Aucore/Ptshell-graphene Nanocatalysts for Fuel Cells. *Advanced Energy Mater.* **2018**, *8*, 1702609.
(22) Jin, D.; Hu, Q.; Neuhauser, D.; von Cube, F.; Yang, Y.; Sachan, R.; Luk, T. S.; Bell, D. C.; Fang, N. X. Quantum Spillover-Enhanced Surface-Plasmonic Absorption at the Interface of Silver and High-Index Dielectrics. *Phys. Rev. Lett.* **2015**, *115*, 193901.
(23) Haiss, W.; Thanh, N. T. K.; Aveyard, J.; Fernig, D. G. Determination of Size and Concentration of Gold Nanoparticles from UV-Vis Spectra. *Anal. Chem.* **2007**, *79*, 4215−4221.
(24) Sardar, R.; Funston, A. M.; Mulvaney, P.; Murray, R. W. Gold Nanoparticles: Past, Present, and Future. *Langmuir* **2009**, *25*, 13840−13851.
(25) Maksymovych, P.; Voznyy, O.; Dougherty, D. B.; Sorescu, D. C.; Yates, J. T., Jr. Gold-adatom as a key structural component in self-assembled monolayers of organosulfur molecules on Au(111). *Prog. Surf. Sci.* **2010**, *85*, 206−240.
(26) Reimers, J. R.; Ford, M. J.; Halder, A.; Ulstrup, J.; Hush, N. S. Gold surfaces and nanoparticles are protected by Au(0)-thiyl species and are destroyed when Au(I)-thiolates form. *Proc. Natl. Acad. Sci. U. S. A.* **2016**, *113*, E1424−E1433.
(27) Reimers, J. R.; Ford, M. J.; Marcuccio, S.; Ulstrup, J.; Hush, N. S. Competition of van der Waals and chemical forces on gold-sulfur surfaces and nanoparticles. *Nat. Rev. Chem.* **2017**, *1*, No. 0017.
(28) Quinn, B. M.; Liljeroth, P.; Ruiz, V.; Laaksonen, T.; Kontturi, K. Electrochemical resolution of 15 oxidation states for monolayer protected gold nanoparticles. *J. Am. Chem. Soc.* **2003**, *125*, 6664−6665.
(29) Laaksonen, T.; Ruiz, V.; Liljeroth, P.; Quinn, B. M. Quantized charging of monolayer-protected nanoparticles. *Chem. Soc. Rev.* **2008**, *37*, 1836−1846.
(30) Chen, S. Discrete Charge Transfer in Nanoparticle Solid Films. *J. Mater. Chem.* **2007**, *17*, 4115−4121.
(31) Sardar, R.; Funston, A. M.; Mulvaney, P.; Murray, R. Gold nanoparticles: Past, present and future. *Langmuir* **2009**, *25*, 13840−13851.
(32) Albrecht, T.; Mertens, S. F. L.; Ulstrup, J. Intrinsic Multi-State Switching of Gold Clusters through Electrochemical Gating. *J. Am. Chem. Soc.* **2007**, *129*, 9162−9167.
(33) Li, Z.; Liu, Y.; Mertens, S. F. L.; Pobelov, I. V.; Wandlowski, T. From redox gating to quantized charging. *J. Am. Chem. Soc.* **2010**, *132*, 8187−8193.
(34) Medvedev, I. G. Single-electron non-adiabatic tunneling through a metal nanoparticle with due account of the solvent dynamic effect: The generalization of the "orthodox" theory. *Electrochem. Commun.* **2011**, *13*, 498−501.
(35) Brodersen, S. H.; Grønbjerg, U.; Hvolbæk, B.; Schøtz, J. Understanding the Catalytic Activity of Gold Nanoparticles through Multiscale Simulations. *J. Catal.* **2011**, *284*, 34−41.
(36) Hvolbæk, B.; Janssens, T. V. W.; Clausen, B. S.; Falsig, H.; Christensen, C. H.; Nørskov, J. K. Catalytic Activity of Au Nanoparticles. *Nano Today* **2007**, *2*, 14−18.
(37) Chi, Q.; Ford, M. J.; Halder, A.; Hush, N. S.; Reimers, J. R.; Ulstrup, J. Sulfur ligand mediated electrochemistry of gold surfaces and nanoparticles: what, how, and why? *Curr. Opin. Electrochemistry* **2017**, *1*, 7−15.
(38) Zhang, J.; Welinder, A. C.; Chi, Q.; Ulstrup, J. Electrochemically Controlled Self-assembled Monolayers Characterized with Molecular and Sub-molecular Resolution. *Phys. Chem. Chem. Phys.* **2011**, *12*, 9999−10011.
(39) Kuznetsov, A.M.; Ulstrup, J. *Electron Transfer in Chemistry and Biology: An Introduction to the Theory*; Wiley: Chichester, 1998.
(40) Kuznetsov, A.M. *Charge Transfer in Physics, Chemistry and Biology*; Gordon and Breach Publishers: Reading, UK, 1995.
(41) (a) Kuznetsov, A. M.; Ulstrup, J. Mechanisms of *In situ* Scanning Tunnelling Microscopy of Organized Redox Molecular Assemblies. *J. Phys. Chem. A* **2000**, *104*, 11531−11540. (b) Errata: *J. Phys. Chem. A 2001*, 105, 7474.
(42) Kuznetsov, A. M.; Medvedev, I. G.; Ulstrup, J. Electrical double layer effect on observable characteristics of the tunnel current through a bridged electrochemical contact. *J. Chem. Phys.* **2007**, *127*, 104708.
(43) Medvedev, I. G. Tunnel current through a redox molecule coupled to classical phonon modes in the strong tunneling limit. *Phys. Rev. B: Condens. Matter Mater. Phys.* **2007**, *76*, 125312.
(44) Zhang, J.; Kuznetsov, A. M.; Medvedev, I. G.; Chi, Q.; Albrecht, T.; Jensen, P. S.; Ulstrup, J. Single-molecule Electron Transfer in Electrochemical Environments. *Chem. Rev.* **2008**, *108*, 2737−2791.
(45) Dogonadze, R. R.; Ulstrup, J.; Kharkats, Yu.I. A Theory of Electrode Reactions through Bridge Transition States. Bridges with a Discrete Electronic Energy Spectrum. *J. Electroanal. Chem. Interfacial Electrochem.* **1972**, *47*, 47−61.
(46) Dogonadze, R. R.; Ulstrup, J.; Kharkats, Yu.I. A Theory of Electrode Reactions through Bridge Transition States. Bridges with a Quasi-continuous Electronic Eenergy Spectrum. *J. Electroanal. Chem. Interfacial Electrochem.* **1973**, *43*, 164−174.
(47) Kuznetsov, A. M.; Ulstrup, J. Dissipative Relaxation of a Low-Energy Intermediate Electronic State in Three-Level Electron Transfer. *Chem. Phys.* **1991**, *157*, 25−33.
(48) Kuznetsov, A. M.; Sommer-Larsen, P.; Ulstrup, J. Resonance and Environmental Fluctuation Effects in STM Currents through Large Adsorbed Molecules. *Surf. Sci.* **1992**, *273*, 52−64.
(49) Chazalviel, J.-N.; Allongue, P. On the origin of the Efficient Nanoparticle Mediated Electron Transfer across a Self-Assembled Monolayer. *J. Am. Chem. Soc.* **2011**, *133*, 762−764.
(50) Kresin, V. V. Collective Resonances and Response Properties of Electrons in Metal Clusters. *Phys. Rep.* **1992**, *220*, 1−52.
(51) Wu, D. Y.; Li, J. F.; Ren, B.; Tian, Z. Q. Electrochemical Surface-enhanced Raman Spectroscopy of Nanostructures. *Chem. Soc. Rev.* **2008**, *37*, 1025−1041.
(52) Zhou, L.; Zacharaiah, M. R. Size Resolved Particle Work Function Measurements of Free Nanoparticles: Aggregates vs Spheres. *Chem. Phys. Lett.* **2012**, *525−526*, 77−81.
(53) Khoa, N. T.; Kim, S. W.; Yoo, D.-H.; Kim, E. J.; Hahn, S. H. Size-Dependent Work Function and Catalytic Performance of Nanoparticles Decorated Graphene Oxide Sheets. *Appl. Catal., A* **2014**, *469*, 159−164.
(54) (a) Kornyshev, A. A.; Kuznetsov, A. M.; Ulstrup, J. Effect of Overpotential on the Electronic Tunnel Factor in Diabatic Electrochemical Processes. *J. Phys. Chem.* **1994**, *98*, 3832−3837. (b) *J. Phys. Chem.* **1994**, *98*, 6664.
(55) Kornyshev, A. A.; Kuznetsov, A. M.; Nielsen, J. U.; Ulstrup, J. Overpotential-induced Labilility of the Electronic Overlap Factor in Long-range Electrochemical Electron Transfer: Charge and Distance Dependence. *Phys. Chem. Chem. Phys.* **2000**, *2*, 141−144.
(56) Dzhavakhidze, P. G.; Kornyshev, A. A.; Tsitsuashvili, G. I. Analytical Solution for the Smith Model for the Neutral and Charged Metal-Surface. *Solid State Commun.* **1984**, *52*, 401−405.

https://dx.doi.org/10.1021/jacs.9b09362
J. Am. Chem. Soc. XXXX, XXX, XXX−XXX

(57) Yu, Y.; Wang, H.; Chen, S. Computational study of bridge-mediated intervalence electron transfer. II. Couplings in different metallocene complexes. *J. Theor. Comput. Chem.* **2012**, *11*, 1341−1356.
(58) Nikitina, V. A.; Kislenko, S. A.; Nazmutdinov, R. R.; Bronshtein, M. D.; Tsirlina, G. A. Ferrocene/ferrocenium Redox Couple at Au(111)/ionic Liquid and Au(111)/acetonitrile Interfaces: A molecular-level View at the Elementary Act. *J. Phys. Chem. C* **2014**, *118*, 6151−6154.
(59) Nazmutdinov, R. R.; Bronshtein, M. D.; Zinkicheva, T. T.; Glukhov, D. V. Modelling of Electron Transfer across Electrochemical Interfaces: State-of-the-art and Challenges for Quantum and Computational Chemistry. *Int. J. Quantum Chem.* **2016**, *116*, 189−201.
(60) Kuznetsov, A. M.; Ulstrup, J. Theory of Electron Transfer at Electrified Interfaces. *Electrochim. Acta* **2000**, *45*, 2339−2361.
(61) Haiss, W.; Albrecht, T.; van Zalinge, H.; Higgins, S. J.; Bethell, D.; Höhenreich, H.; Schiffrin, D. J.; Nichols, R. J.; Kuznetsov, A. M.; Zhang, J.; Chi, Q.; Ulstrup, J. Single-Molecule Conductance of Redox Molecules in Electrochemical Sscanning Tunnelling Microscopy. *J. Phys. Chem. B* **2007**, *111*, 6703−6712.
(62) Datta, S. *Electronic Transport in Mesoscopic Systems*; Cambridge University Press: Cambridge, UK, 1995.
(63) Gao, Yi; Marcus, R. A. On the Theory of Electron Transfer Reactions at Semiconductor/Liquid Interfaces. II. A Free Electron Model. *J. Chem. Phys.* **2000**, *113*, 6351−6360.
(64) Smalley, J. F.; Newton, M. D.; Feldberg, S. W. A simple comparison of interfacial electron transfer rates for surface attached and bulk solution dissolved redox moieties. *J. Electroanal. Chem.* **2008**, *589*, 1−6.
(65) Newton, M. D.; Smalley, J. F. Interfacial bridge-mediated electron transfer: mechanistic analysis based on electrochemical kinetics and theoretical modeling. *Phys. Chem. Chem. Phys.* **2007**, *9*, 555−572.
(66) Zakaraya, M. G.; Ulstrup, J. Theory of dynamic solvent effects on Raman scattering and resonance profiles of polyatomic molecules in solution. *Chem. Phys.* **1989**, *135*, 49−73.
(67) Kharkats, Yu. I.; Ulstrup, J. Resonance effects in three-centre long-range electron transfer. *Chem. Phys. Lett.* **1991**, *182*, 81−87.
(68) Welinder, A. C.; Zhang, J.; Hansen, A. G.; Moth-Poulsen, K.; Christensen, H. E. M.; Kuznetsov, A. M.; Bjørnholm, T.; Ulstrup, J. Voltammetry and electrocatalysis of *Achromobacter xylosoxidans* copper nitrite reductase on functionalized Au(111)-electrode surfaces. *Z. Phys. Chem.* **2007**, *221*, 1343−1378.
(69) Climent, V.; Zhang, J.; Friis, E. P.; Østergaard, L. H.; Ulstrup, J. Voltammetry and in situ scanning tunneling microscopy of laccases and bilirubin oxidase in electrocatalytic dioxygen. reduction on Au(111) single-crystal electrodes. *J. Phys. Chem. C* **2012**, *116*, 1232−1243.
(70) (a) Kuznetsov, A. M.; Ulstrup, J. Mechanisms of in situ scanning tunnelling microscopy of organized redox molecular assemblies. *J. Phys. Chem. A* **2000**, *104*, 11531−11540. (b) Errata: *J. Phys. Chem. A 2001,105*, 7494−7494.
(71) Davydov, A. S. *Quantum Mechanics*; Pergamon Press: Oxford, 1965.
(72) Frisch, M. J.; Trucks, G. W.; Schlegel, H. B.; Scuseria, G. E.; Robb, M. A.; Cheeseman, J. R.; Scalmani, G.; Barone, V.; Petersson, G. A.; Nakatsuji, H.; Li, X.; Caricato, M.; Marenich, A. V.; Bloino, J.; Janesko, B. G.; Gomperts, R.; Mennucci, B.; Hratchian, H. P.; Ortiz, J. V.; Izmaylov, A. F.; Sonnenberg, J. L.; Williams-Young, D.; Ding, F.; Lipparini, F.; Egidi, F.; Goings, J.; Peng, B.; Petrone, A.; Henderson, T.; Ranasinghe, D.; Zakrzewski, V. G.; Gao, J.; Rega, N.; Zheng, L. G. W.; Hada, M.; Ehara, M.; Toyota, K.; Fukuda, R.; Hasegawa, J.; Ishida, M.; Nakajima, T.; Honda, Y.; Kitao, O.; Nakai, H.; Vreven, T.; Throssell, K.; Montgomery, J. A., Jr.; Peralta, J. E.; Ogliaro, F.; Bearpark, M. J.; Heyd, J. J.; Brothers, E. N.; Kudin, K. N.; Staroverov, V. N.; Keith, T. A.; Kobayashi, R.; Raghavachari, J. K.; Rendell, A. P.; Burant, J. C.; Iyengar, S. S.; Tomasi, J.; Cossi, M.; Millam, J. M.; Klene, M.; Adamo, C.; Cammi, R.; Ochterski, J. W.; Martin, R. L.; Morokuma, K.; Farkas, O.; Foresman, J. B.; Fox, D. J. *Gaussian 09*, Revision B.01; Gaussian, Inc.: Wallingford, CT, 2009, 2016.
(73) Hay, P. J.; Wadt, W. R. Ab Initio Effective Core Potentials for Molecular Calculations. Potentials from K to Au Including the Outermost Core Orbitals. *J. Chem. Phys.* **1985**, *82*, 270−283.
(74) Grua, P.; Morreeuw, J. P.; Bercegol, H. Kinetic study of laser damage initiation by creation of an electron plasma from absorbing nanoinclusions. In *Proc. SPIE*. 2002; Vol. 4679, pp 293−302.
(75) Itskovitch, E. M.; Ulstrup, J.; Vorotyntsev, M.A. Ultraviolet and Visible Light Absorption of Solute Molecules in Condensed Media, Chapter 6. In *The Chemical Physics of Solvation. Part B. Spectroscopy of Solvation*; Dogonadze, R. R.; Kálmán, E.; Kornyshev, A. A.; Ulstrup, J., Eds.; Elsevier: Amsterdam, 1986; pp 223−310.
(76) Kubo, R.; Toyozawa, Y. Application of the Method of Generating Function to Radiative and Non-radiative Transitions of a Trapped Electron in a Crystal. *Prog. Theor. Phys.* **1955**, *13*, 160−182.
(77) Dogonadze, R. R.; Kuznetsov, A. M.; Vorotyntsev, M. A. Theory of Highly Exothermic Electron-Transfer Processes. *Z. Phys. Chem.* **1976**, *100*, 1−16.
(78) Kjaer, A. M.; Ulstrup, J. Solvent Bandwidth Dependence and Band Asymmetry Features of Charge Transfer Transitions in N-pyridinium Phenolates. *J. Am. Chem. Soc.* **1987**, *109*, 1934−1942.
(79) Marcus, R. A. Theory of Oxidation-Reduction Reactions Involving Electron Transfer. Part 4. − Statistical-Mechanical Basis for Treating Contributions from Solvent, Ligands, and Inert Salt. *Discuss. Faraday Soc.* **1960**, *29*, 21−31.
(80) Van Duyne, R. P.; Fischer, S. F. Nonadiabatic Description of Electron-transfer Reactions Involving Large Free-energy Changes. *Chem. Phys.* **1974**, *5*, 183−197.
(81) Ulstrup, J.; Jortner, J. The Effect of Intramolecular Quantum Modes on Free Energy Relationships for Electron Transfer Reactions. *J. Chem. Phys.* **1975**, *63*, 4358−4368.
(82) Gundlach, L.; Willig, F. Ultrafast Photoinduced Electron Transfer at Electrodes: The General Case of a Heterogeneous Electron-Transfer Reaction. *ChemPhysChem* **2012**, *13*, 2877−2881.
(83) Nazmutdinov, R. R.; Berezin, A. S.; Soldano, G. J.; Schmickler, W. Orbital Overlap Effects in Electron Transfer Reactions Across a Metal Nanowire/Electrolyte Solution Interface. *J. Phys. Chem. C* **2013**, *117*, 13021−13027.
(84) Kurelchuk, U. N.; Borisyuk, P. V.; Vasilyev, O. S.; Lebedinsky, Yu.Yu. Investigation of the Electronic Properties of the Surface and Bulk Forms of Gold and Palladium. *J. Phys.: Conf. Ser.* **2017**, *941*, No. 012110.
(85) Evenson, J. E.; Karplus, M. Effective Coupling in Bridged Electron Transfer Molecules: Computational Formulation and Examples. *J. Chem. Phys.* **1992**, *96*, 5272−5278.
(86) Hsu, C.-P.; Marcus, R. A. A sequential formula for electronic coupling in long range bridge assisted electron transfer: formulation of theory and application to alkanethiol monolayers. *J. Chem. Phys.* **1997**, *106*, 584−597.
(87) Newton, M. D.; Smalley, J. F. Interfacial bridge-mediated electron transfer: mechanistic analysis based on electrochemical kinetics and theoretical modeling. *Phys. Chem. Chem. Phys.* **2007**, *9*, 555−572.
(88) Kislenko, S. A.; Nikitina, V. A.; Nazmutdinov, R. R. When do defectless alkanethiol SAMs in ionic liquids become penetrable? A molecular dynamics study. *Phys. Chem. Chem. Phys.* **2015**, *17*, 31947−31955.
(89) Liu, Y.-P.; Newton, M. D. Reorganisation energy for electron transfer at film-modified electrode surfaces: a dielectric continuum model. *J. Phys. Chem.* **1994**, *98*, 7162−7169.
(90) Khruschcheva, M. L.; Tsirlina, G. A.; Petrij, O. A. Dependence of the absolute rate constant of an electrochemical process on the metal structure: Electroreduction of the Cr(3+) ethylene diamine tetraacetate on Hg, Bi, and Cd and its analysis in the context of the classical approach. *Russ. J. Electrochem.* **1998**, *34*, 325−333.
(91) Koene, L.; Sluyters-Rehbach, M.; Sluyters, J. H. Electrode kinetics and the nature of the metal electrode. 1. Zn^{2+} reduction from

https://dx.doi.org/10.1021/jacs.9b09362
J. Am. Chem. Soc. XXXX, XXX, XXX−XXX

aqueous 1 M $NaClO_4$ solution at indium and thallium amalgams of varied composition. *J. Electroanal. Chem.* **1996**, *402*, 57−72.
(92) Kuznetsov, A.M.; Ulstrup, J. Environmental modulation of the electronic factor in electron transfer rate theory, and implications for the primary steps in bacterial photosynthesis. In *Tunneling, The Jerusalem Symposia on Quantum Chemistry and Biochemistry*; Jortner, J.; Pullman, B., Eds.; D. Reidel: Dordrecht, 1986; Vol. *19*, pp 345−360.

https://dx.doi.org/10.1021/jacs.9b09362
J. Am. Chem. Soc. XXXX, XXX, XXX−XXX